Article

Synthesis and Characterization of Li[(NiCoMn)(NiMn)]O with the Microscale Core–Shell Structure as the Positive Electrode Material for Lithium Batteries

Yang-Kook Sun, Seung-Taek Myung, Myung-Hoon Kim, Jai Prakash, and Khalil Amine

J. Am. Chem. Soc., **2005**, 127 (38), 13411-13418• DOI: 10.1021/ja053675g • Publication Date (Web): 31 August 2005

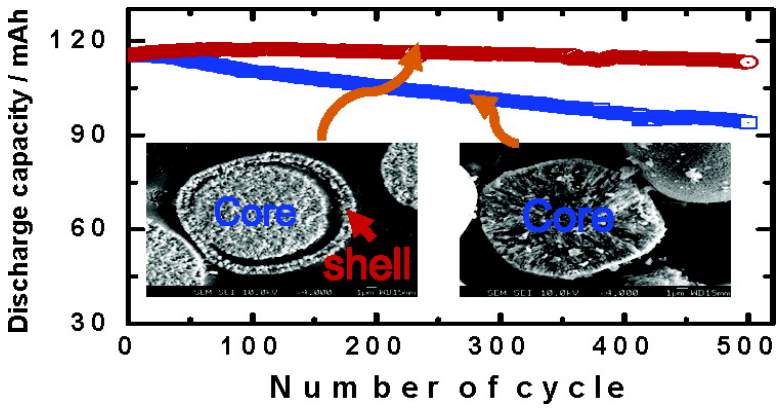

More About This Article

Additional resources and features associated with this article are available within the HTML version:

- Supporting Information
- Links to the 11 articles that cite this article, as of the time of this article download
- Access to high resolution figures
- Links to articles and content related to this article
- Copyright permission to reproduce figures and/or text from this article

View the Full Text HTML

J|A|C|S
ARTICLES
Published on Web 08/31/2005

Synthesis and Characterization of $Li[(Ni_{0.8}Co_{0.1}Mn_{0.1})_{0.8}(Ni_{0.5}Mn_{0.5})_{0.2}]O_2$ with the Microscale Core−Shell Structure as the Positive Electrode Material for Lithium Batteries

Yang-Kook Sun,*,† Seung-Taek Myung,‡ Myung-Hoon Kim,† Jai Prakash,§ and Khalil Amine||

Contribution from the Center for Information and Communication Materials, Department of Chemical Engineering, Hanyang University, Seoul 133-791, Korea, Department of Frontier Materials and Functional Engineering, Graduate School of Engineering, Iwate University, Iwate 020-8551, Japan, Department of Chemical and Environmental Engineering, Illinois Institute of Technology, Chicago, Illinois 60616, and Electrochemical Technology Program, Chemical Engineering Division, Argonne National Laboratory, 9700 South Cass Avenue, Argonne, Illinois 60439

Received June 20, 2005; E-mail: yksun@hanyang.ac.kr

Abstract: The high capacity of Ni-rich $Li[Ni_{1-x}M_x]O_2$ (M = Co, Mn) is very attractive, if the structural instability and thermal properties are improved. $Li[Ni_{0.5}Mn_{0.5}]O_2$ has good thermal and structural stabilities, but it has a low capacity and rate capability relative to the Ni-rich $Li[Ni_{1-x}M_x]O_2$. We synthesized a spherical core−shell structure with a high capacity (from the $Li[Ni_{0.8}Co_{0.1}Mn_{0.1}]O_2$ core) and a good thermal stability (from the $Li[Ni_{0.5}Mn_{0.5}]O_2$ shell). This report is about the microscale spherical core−shell structure, that is, $Li[Ni_{0.8}Co_{0.1}Mn_{0.1}]O_2$ as the core and a $Li[Ni_{0.5}Mn_{0.5}]O_2$ as the shell. A high capacity was delivered from the $Li[Ni_{0.8}Co_{0.1}Mn_{0.1}]O_2$ core, and a high thermal stability was achieved by the $Li[Ni_{0.5}Mn_{0.5}]O_2$ shell. The core−shell structured $Li[(Ni_{0.8}Co_{0.1}Mn_{0.1})_{0.8}(Ni_{0.5}Mn_{0.5})_{0.2}]O_2$/carbon cell had a superior cyclability and thermal stability relative to the $Li[Ni_{0.8}Co_{0.1}Mn_{0.1}]O_2$ at the 1 C rate for 500 cycles. The core−shell structured $Li[(Ni_{0.8}Co_{0.1}Mn_{0.1})_{0.8}(Ni_{0.5}Mn_{0.5})_{0.2}]O_2$ as a new positive electrode material is a significant breakthrough in the development of high-capacity lithium batteries.

Introduction

Ni-rich $Li[Ni_{1-x}M_x]O_2$ (M = metals) have attracted much interest as lithium storage materials for rechargeable lithium batteries because of their low cost and high capacity.[1−3] The substitutions of Ni with Co and/or Mn improve the structural stability upon cycling. Such improvements result from the reduced phase transition from hexagonal to monoclinic that causes a NiO layer distortion in the highly delithiated state, compared to $LiNiO_2$.[4] The electrodes based on the chemical formula $Li_{1-\delta}[Ni_{1-x}M_x]O_2$ are structurally unstable during thermal runaway reactions due to the oxygen release from the host structure. The released oxygen can then react with the organic electrolyte and carbon anode causing flame and severe safety problems. These problems have hindered their commercial use in a lithium battery system, though they have much higher specific capacity than $LiCoO_2$ in the same voltage range (3.0−4.3 V).[5]

Ohzuku and Makimura recently introduced a new cathode material, $Li[Ni_{0.5}Mn_{0.5}]O_2$.[6] The chemistry of this material is interesting; it is different from $LiNiO_2$ (with an average Ni oxidation state of +3) and from the formal charges of Ni (+2) and Mn (+4) in $Li[Ni_{0.5}Mn_{0.5}]O_2$.[7] In this case, the average oxidation state of Mn is tetravalent, so that the electrochemically inactive tetravalent Mn provides significant structural stability and results in a simple topotactic reaction maintaining the hexagonal phase during electrochemical cycling, even at the

† Hanyang University.
‡ Iwate University.
§ Illinois Institute of Technology.
|| Argonne National Laboratory.

(1) Thomas, M. G. S. R.; David, W. I. F.; Goodenough, J. B.; Groves, P. Synthesis and structural characterization of the normal spinel $Li[Ni_2]O_4$. *Mater. Res. Bull.* **1985**, *20*, 1137−1146.
(2) Broussely, M.; Perton, F.; Biensan, Ph.; Bodet, J. M.; Lecerf, A.; Delmas, C.; Rougier, A.; Pérès, J. P. Li_xNiO_2, A promising cathode for rechargeable lithium batteries. *J. Power Sources* **1995**, *54*, 109−114.
(3) Delmas, C.; Prado, G.; Rougier, A.; Suard, E.; and Fournès, L. Effect of iron on the electrochemical behaviour of lithium nickelate: from $LiNiO_2$ to 2D-$LiFeO_2$. *Solid State Ionics* **2000**, *135*, 71−79.
(4) Li, W.; Reimers, J. N.; Dahn, J. R. In situ X-ray diffraction and electrochemical studies of $Li_{1-x}NiO_2$. *Solid State Ionics* **1993**, *67*, 123−130.
(5) Arai, H.; Okada, S.; Sakurai, Y.; Yamaki, J. Thermal behavior of $Li_{1-y}NiO_2$ and the decomposition mechanism. *Solid State Ionics* **1998**, *109*, 295−302.
(6) Ohzuku, T.; Makimura, Y. Layered lithium insertion material of $LiNi_{1/2}Mn_{1/2}O_2$: A possible alternative to $LiCoO_2$ for advanced lithium-ion batteries. *Chem. Lett.* **2001**, *30*, 744−745.
(7) Yoon, W.-S.; Paik, Y.; Yang, X.-Q.; Balasubramanian, M.; McBreen, J.; Grey, C. P. Investigation of the local structure of the $LiNi_{0.5}Mn_{0.5}O_2$ cathode material during electrochemical cycling by X-ray absorption and NMR spectroscopy. *Electrochem. Solid State Lett.* **2002**, *5*, A263−A266.

high voltage cutoff limit of 4.6 V.[8−10] Due to its improved structural stability, the onset of the exothermal temperature by $Li_{1-\delta}[Ni_{0.5}Mn_{0.5}]O_2$ is usually as high as 280 °C, and the heat generation at that temperature is less than Ni-rich $Li_{1-\delta}[Ni_{1-x}M_x]O_2$ (M = metals).[11,12] Even though the $Li[Ni_{0.5}Mn_{0.5}]O_2$ compound has several advantages, the poor rate capability should be improved for use as a Li^+ intercalation material in a lithium ion battery.[13]

We expected that the two materials described above would have synergetic effects, that is, a high capacity for $Li[Ni_{0.8}Co_{0.1}Mn_{0.1}]O_2$ and a good thermal stability for $Li[Ni_{0.5}Mn_{0.5}]O_2$. To achieve these desired properties, a spherical core−shell structure was developed, using $Li[Ni_{0.8}Co_{0.1}Mn_{0.1}]O_2$ as the core and $Li[Ni_{0.5}Mn_{0.5}]O_2$ as the shell. We postulated that a higher capacity would be delivered from the $Li[Ni_{0.8}Co_{0.1}Mn_{0.1}]O_2$ core and a greater thermal stability would be achieved by the $Li[Ni_{0.5}Mn_{0.5}]O_2$ shell. Cho et al.[14,15] suggested that thin coating layers (≤10 nm) of Al_2O_3- and $AlPO_4$-coated $LiCoO_2$ and $Li[Ni_{0.8}Co_{0.1}Mn_{0.1}]O_2$ were effective with respect to the capacity and thermal stability. However, such coatings do not seem to suppress the structural change during electrochemical cycling (as was observed by in situ XRD studies[16]) because it is likely that the thin layer itself, which is composed of an amorphous or low crystalline phase, cannot preserve the structural change from the hexagonal to monoclinic phases of the active materials. For this reason, it is only possible to suppress the structural changes if a thick shell (micrometer order) completely encapsulates the core.

The fabrication of the spherical core−shell structure particles with hollow interiors has attracted considerable attention in recent years because of the particles' potential use as low-density capsules for photonic crystals, catalysts, diagnostics, pharmacology, etc.[17−20] A number of synthetic methods were developed for the synthesis of core−shell structured powders: interface assembly strategies,[21,22] the layer-by-layer self-assembly process,[23] hydrothermal precipitation method,[24] and the template method.[25] Nanometer- and submicrometer-sized core-structure particles with spherical shapes were effectively produced using the above preparation methods.[18−25] The core−shell structure exhibits many interesting properties.

Scheme 1. Schematic Drawing of Formation Process of Microscale Core−Shell Structured $Li[(Ni_{0.8}Co_{0.1}Mn_{0.1})_{1-x}(Ni_{0.5}Mn_{0.5})_x]O_2$

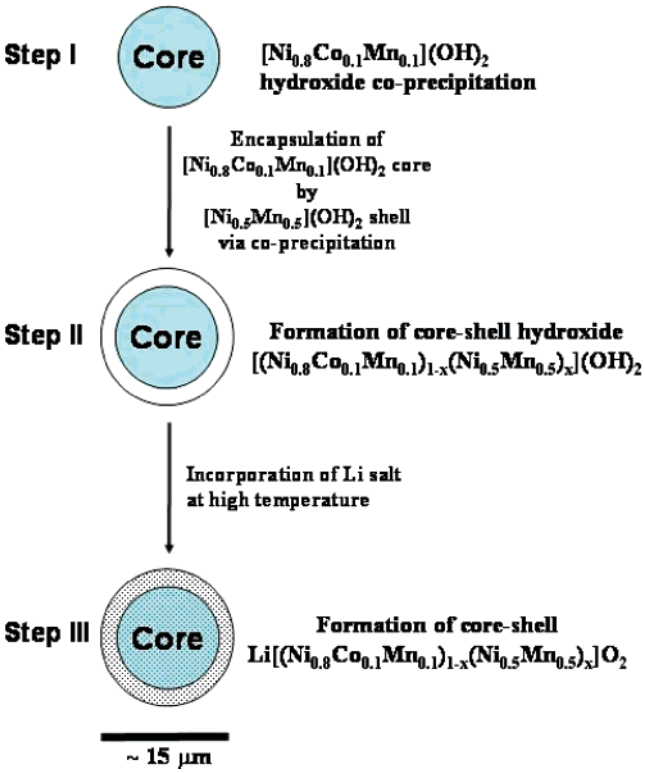

For lithium battery applications, however, a high-density active material is required to achieve a higher energy density because the inner space of a battery is limited. For this reason, we postulated that the coprecipitation method is one of the best approaches to synthesize spherical core−shell structure particles with high interior and exterior densities. Recently, we reported the optimized synthesis of spherical, dense $Li[Ni_{1/3}Co_{1/3}Mn_{1/3}]O_2$ powders via coprecipitation.[26] Scheme 1 shows our ideas for the core−shell structured particles. First, $[Ni_{0.8}Co_{0.1}Mn_{0.1}](OH)_2$ is formed as the core, with a particle size of about 12−13 μm in diameter. The core is then completely encapsulated by a $[Ni_{0.5}Mn_{0.5}](OH)_2$ shell with a thickness between 1 and 1.5 μm (Step II of Scheme 1). Finally, the calcination of the core−shell hydroxide and lithium salt gives rise to the formation of

(8) Yang, X.-Q.; McBreen, J.; Yoon, W.-S.; Grey, C. P. Crystal structure changes of $LiMn_{0.5}Ni_{0.5}O_2$ cathode materials during charge and discharge studied by synchrotron based in situ XRD. *Electrochem. Commun.* **2002**, *4*, 649−954.
(9) Myung, S.-T.; Komaba, S.; Hosoya, K.; Hirosaki, N.; Miura, U.; Kumagai, N. Synthesis of $LiNi_{0.5}Mn_{0.5-x}Ti_xO_2$ by an emulsion drying method and effect of Ti on structure and electrochemical properties. *Chem. Mater.* **2005**, *17*, 2427−2435.
(10) Lu, Z.; Beaulieu, L. Y.; Donaberger, R. A.; Thomas, C. L.; Dahn, J. R. Synthesis, structure, and electrochemical behavior of $Li[Ni_xLi_{1/3-2x/3}Mn_{2/3-x/3}]O_2$. *J. Electrochem. Soc.* **2002**, *149*, A778−A791.
(11) Kang, S.-H.; Kim, J.; Stoll, M. E.; Abraham, D.; Sun, Y.-K.; Amine, K. Layered $Li(Ni_{0.5-x}Mn_{0.5-x}M_{2x}')O_2$ (M′ = Co, Al, Ti; $x = 0$, 0.025) cathode materials for Li-ion rechargeable batteries. *J. Power Sources* **2002**, *112*, 41−48.
(12) Jouanneau, S.; MacNeil, D. D.; Lu, Z.; Beattie, S. D.; Murphy, G.; Dahn, J. R. Morphology and safety of $Li[Ni_xCo_{1-2x}Mn_x]O_2$ ($0 \le x \le 1/2$). *J. Electrochem. Soc.* **2003**, *150*, A1299−A1304.
(13) Makimura, Y.; Ohzuku, T. Lithium insertion material of $LiNi_{1/2}Mn_{1/2}O_2$ for advanced lithium-ion batteries. *J. Power Sources* **2003**, *119−121*, 156−160.
(14) Cho, J.; Kim, Y.-J.; Kim. T.-J.; Park, B. Zero-strain intercalation cathode for rechargeable Li-ion cell. *Angew. Chem., Int. Ed.* **2001**, *40*, 3367−3369.
(15) Cho, J.; Kim, T.-J.; Kim, J.; Noh, M.; Park, B. Synthesis, thermal, and electrochemical properties of $AlPO_4$-coated $LiNi_{0.8}Co_{0.1}Mn_{0.1}O_2$ cathode material for a Li-ion cell. *J. Electrochem. Soc.* **2004**, *151*, A1899−A1904.
(16) Chen, Z.; Dahn, J. R. Effect of a ZrO_2 coating on the structure and electrochemistry of Li_xCoO_2 when cycled to 4.5 V. *Electrochem. Solid State Lett.* **2002**, *5*, A213−A216.
(17) Schartl, W. Cross-linked spherical nanoparticles with core−shell topology. *Adv. Mater.* **2000**, *12*, 1899−1908.
(18) Caruso, F. Nanoengineering of particle surfaces. *Adv. Mater.* **2001**, *13*, 11−22.
(19) Mandal, T. K.; Fleming, M. S.; Walt, D. R. Production of hollow polymeric microspheres by surface-confined living radical polymerization on silica templates. *Chem. Mater.* **2000**, *12*, 3481−3487.
(20) Suryanarayanan, V.; Nair A. S.; Tom, R. T.; Pradeep, T. Porosity of core−shell nanoparticles. *J. Mater. Chem.* **2004**, *14*, 2661−2666.
(21) Nakashima, T.; Kimizuka, N. Interfacial synthesis of hollow TiO_2 microspheres in ionic liquids. *J. Am. Chem. Soc.* **2003**, *125*, 6386−6387.
(22) Hu, J.-S.; Guo, Y.-G.; Liang, H.-P.; Wan, L.-J.; Bai, C.-L.; Wang, Y.-G. Interface assembly synthesis of inorganic composite hollow spheres. *J. Phys. Chem. B* **2004**, *108*, 9734−9738.
(23) Caruso, F.; Spasova, M.; Susha, A.; Giersig. M.; Caruso, R. A. Magnetic nanocomposite particles and hollow spheres constructed by a sequential layering approach. *Chem. Mater.* **2001**, *13*, 109−118.
(24) Guo, C.-W.; Cao, Y.; Xie, S.-H.; Dai, W.-L.; Fan, K.-N. Fabrication of mesoporous core−shell structured titania microspheres with hollow interiors. *Chem. Commun.* **2003**, 700−701.
(25) Zhang, Y.; Li, G.; Zhang, L. Synthesis of indium hollow spheres and nanotubes by a simple template-free solvothermal process. *Inorg. Chem. Commun.* **2004**, *7*, 344−346.
(26) Lee, M.-H.; Kang, Y.-J.; Myung, S.-T.; Sun, Y.-K. Synthetic optimization of $Li[Ni_{1/3}Co_{1/3}Mn_{1/3}]O_2$ via co-precipitation. *Electrochim. Acta* **2004**, *50*, 939−948.

spherical core−shell Li[(Ni$_{0.8}$Co$_{0.1}$Mn$_{0.1}$)$_{1-x}$(Ni$_{0.5}$Mn$_{0.5}$)$_x$]O$_2$ powders (Step III), of which Li[Ni$_{0.8}$Co$_{0.1}$Mn$_{0.1}$]O$_2$ exists as the core and Li[Ni$_{0.5}$Mn$_{0.5}$]O$_2$ appears as the shell.

Experimental Section

Synthesis and Analysis of Metal Contents. [Ni$_{0.8}$Co$_{0.1}$Mn$_{0.1}$](OH)$_2$ and [(Ni$_{0.8}$Co$_{0.1}$Mn$_{0.1}$)$_{1-x}$(Ni$_{0.5}$Mn$_{0.5}$)$_x$](OH)$_2$ compounds were synthesized by the coprecipitation method. The appropriate amounts of NiSO$_4$·6H$_2$O, CoSO$_4$·7H$_2$O, and MnSO$_4$·H$_2$O (cationic ratio of Ni:Co:Mn = 8:1:1) were used as the starting materials for [Ni$_{0.8}$Co$_{0.1}$Mn$_{0.1}$](OH)$_2$. They were pumped into a continuously stirred tank reactor (CSTR, capacity 4 L) in a nitrogen atmosphere. At the same time, a 2.0 mol/dm^3 NaOH solution (aq) and the desired amount of NH$_4$OH solution (aq) as the chelating agent were also separately fed into the reactor. The concentration of the solution, pH, temperature, and stirring speed of the mixture in the reactor were carefully controlled. To synthesize the core−shell structured [(Ni$_{0.8}$Co$_{0.1}$Mn$_{0.1}$)$_{1-x}$(Ni$_{0.5}$Mn$_{0.5}$)$_x$](OH)$_2$, the resulting spherical [Ni$_{0.8}$Co$_{0.1}$Mn$_{0.1}$](OH)$_2$ was continuously reacted with NiSO$_4$·6H$_2$O and MnSO$_4$·H$_2$O (cationic ratio of Ni:Mn = 1:1). These [Ni$_{0.8}$Co$_{0.1}$Mn$_{0.1}$](OH)$_2$ and [(Ni$_{0.8}$Co$_{0.1}$Mn$_{0.1}$)$_{1-x}$(Ni$_{0.5}$Mn$_{0.5}$)$_x$](OH)$_2$ compounds were thoroughly mixed with LiOH·H$_2$O and heated at 750 °C for 12 h and 770 °C for 20 h in air, respectively. The chemical compositions of the resulting powders were analyzed by atomic absorption spectroscopy (AAS, Vario 6, Analyticjena).

XRD, SEM, and XPS. Powder X-ray diffraction (XRD, Rint-2000, Rigaku, Japan) measurements using Cu Kα radiation were employed to identify the crystalline phase of the synthesized materials. XRD data were obtained at $2\theta = 10-80°$, with a step size of 0.03° and a count time of 5 s. From the XRD data, the lattice parameters were calculated by the least-squares method. The morphology and atomic concentration of powders were observed using a scanning electron microscope with an energy dispersive spectroscope (SEM, JSM 6400, JEOL, Japan). X-ray photoelectron spectroscopy (XPS, PHI 5600, Perkin-Elmer) measurements were performed to obtain information about the surface of Li[(Ni$_{0.8}$Co$_{0.1}$Mn$_{0.1}$)$_{1-x}$(Ni$_{0.5}$Mn$_{0.5}$)$_x$]O$_2$. Macromode (about 3 mm × 3 mm) Ar ion etching was used to examine the concentration depth profiles of the coated powders. The etching rate was estimated to be 1.5 nm/min.[1]

Electrochemical Tests. The prepared powders were mixed with carbon black and polyvinylidene fluoride (80:10:10) in *N*-methylpyrrolidinone to fabricate the positive electrodes. The obtained slurry was coated onto Al foil and roll-pressed at 120 °C in air. The electrodes were dried overnight at 120 °C in a vacuum prior to use. Preliminary cell tests were done using the 2032 coin-type cell with Li metal as the negative electrode. The long cycle-life tests were performed in a laminated-type full cell wrapped with an Al pouch (thickness = 1.5 mm, width = 40 mm, and length = 60 mm, capacity = 120 mAh). Mesocarbon microbeads (MCMB, Osaka gas) were used as the negative electrode. The electrolyte solution was 1 M LiPF$_6$ in ethylene carbonate−diethyl carbonate (1:1 in volume). The fabrication of the cell was done in a dry room. A cell formation was performed for the Li ion cell; three cycles were performed at room temperature at the 0.1, 0.2, and 0.5 C rates in the voltage range of 3.0−4.3 V. The C rate is defined as the exchange of 0.5 F per formula unit in 1 h. The cells, then, were charged and discharged between 3.0 and 4.3 V by applying a constant 1 C current at 25 °C.

DSC. For the differential scanning calorimetry (DSC) experiments, the Li ion cells were fully charged to 4.3 V and opened in an Ar-filled dry room. After the remaining electrolyte was carefully removed from the surface of the electrode, the positive electrode materials were recovered from the current collector. A stainless steel sealed pan with a gold-plated copper seal was used to collect 3−5 mg samples. Measurements were carried out in a Pyris 1 differential scanning calorimeter (Perkin-Elmer Corp., Germany) using a temperature scan rate of 1 °C/min.

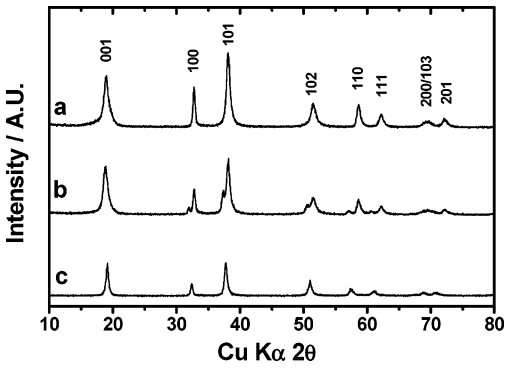

Figure 1. XRD patterns of as-prepared (a) pristine [Ni$_{0.8}$Co$_{0.1}$Mn$_{0.1}$](OH)$_2$, (b) [(Ni$_{0.8}$Co$_{0.1}$Mn$_{0.1}$)$_{0.8}$(Ni$_{0.5}$Mn$_{0.5}$)$_{0.2}$](OH)$_2$, and (c) [Ni$_{0.5}$Mn$_{0.5}$](OH)$_2$. The synthesis of the hydroxide was carried out using coprecipitation method.

Results and Discussion

Though Li[Ni$_{0.5}$Mn$_{0.5}$]O$_2$ has good structural and thermal stabilities, its poor rate capability would affect the electrochemical properties of the spherical core−shell Li[(Ni$_{0.8}$Co$_{0.1}$Mn$_{0.1}$)$_{1-x}$(Ni$_{0.5}$Mn$_{0.5}$)$_x$]O$_2$ powders if the shell is too thick. Therefore, the thickness of the shell was controlled to 1−1.5 μm. Scheme 1 shows the schematics for the synthesis of the core−shell structured Li[(Ni$_{0.8}$Co$_{0.1}$Mn$_{0.1}$)$_{1-x}$(Ni$_{0.5}$Mn$_{0.5}$)$_x$]O$_2$. We first prepared the [Ni$_{0.8}$Co$_{0.1}$Mn$_{0.1}$](OH)$_2$ by the coprecipitation method. The prepared [Ni$_{0.8}$Co$_{0.1}$Mn$_{0.1}$](OH)$_2$ had a typical structure of layered M(OH)$_2$ (Figure 1a).[27] The SEM images of Figure 2a and b show that the synthesized [Ni$_{0.8}$Co$_{0.1}$Mn$_{0.1}$](OH)$_2$ material had a spherical morphology, and the average particle size was estimated to almost 12−13 μm in diameter. The Ni and Mn solution was then continuously pumped into the coprecipitation reactor, where [Ni$_{0.8}$Co$_{0.1}$Mn$_{0.1}$](OH)$_2$ had already precipitated due to the contamination of the prepared [Ni$_{0.8}$Co$_{0.1}$Mn$_{0.1}$](OH)$_2$ with O$_2$ in the air, and finally the [Ni$_{0.5}$Mn$_{0.5}$](OH)$_2$ piled on the surface of [Ni$_{0.8}$Co$_{0.1}$Mn$_{0.1}$](OH)$_2$. [Ni$_{0.5}$Mn$_{0.5}$](OH)$_2$ was also prepared for comparison. Figure 1b shows the XRD pattern of [(Ni$_{0.8}$Co$_{0.1}$Mn$_{0.1}$)$_{1-x}$(Ni$_{0.5}$Mn$_{0.5}$)$_x$](OH)$_2$. The XRD shows two diffraction patterns of the [Ni$_{0.8}$Co$_{0.1}$Mn$_{0.1}$](OH)$_2$ and [Ni$_{0.5}$Mn$_{0.5}$](OH)$_2$ phases.

SEM images shown in Figure 2c and d show that the particle shape was spherical and the estimated average particle size of the [(Ni$_{0.8}$Co$_{0.1}$Mn$_{0.1}$)$_{1-x}$(Ni$_{0.5}$Mn$_{0.5}$)$_x$](OH)$_2$ was approximately 15 μm in diameter. In addition, a closer inspection of Figures 2f clearly indicates the existence of core−shell structure. The core−shell structured hydroxide had larger particles than [Ni$_{0.8}$Co$_{0.1}$Mn$_{0.1}$](OH)$_2$ because the shell covers the pristine [Ni$_{0.8}$Co$_{0.1}$Mn$_{0.1}$](OH)$_2$, as anticipated. The chemical composition of the prepared core−shell powders was [Ni$_{0.74}$Co$_{0.08}$Mn$_{0.18}$](OH)$_2$, which was determined from atomic absorption spectroscopy (AAS), and can be written as [(Ni$_{0.8}$Co$_{0.1}$Mn$_{0.1}$)$_{0.8}$(Ni$_{0.5}$Mn$_{0.5}$)$_{0.2}$](OH)$_2$. To directly observe the existence of the shell and the thickness of the synthesized [Ni$_{0.8}$Co$_{0.1}$Mn$_{0.1}$](OH)$_2$ and [(Ni$_{0.8}$Co$_{0.1}$Mn$_{0.1}$)$_{0.8}$(Ni$_{0.5}$Mn$_{0.5}$)$_{0.2}$](OH)$_2$, the powders were partially broken into small pieces in an agate mortar, and the corresponding SEM images are in Figure 2e and f, respectively. For the [Ni$_{0.8}$Co$_{0.1}$Mn$_{0.1}$](OH)$_2$, the cross-section image shows a simple secondary particle structure with no core−shell structure. The image of [(Ni$_{0.8}$Co$_{0.1}$Mn$_{0.1}$)$_{0.8}$(Ni$_{0.5}$Mn$_{0.5}$)$_{0.2}$](OH)$_2$ clearly shows that the material is composed of

(27) Joint Committee on Powder Diffraction Standards, Card No. 14-0117.

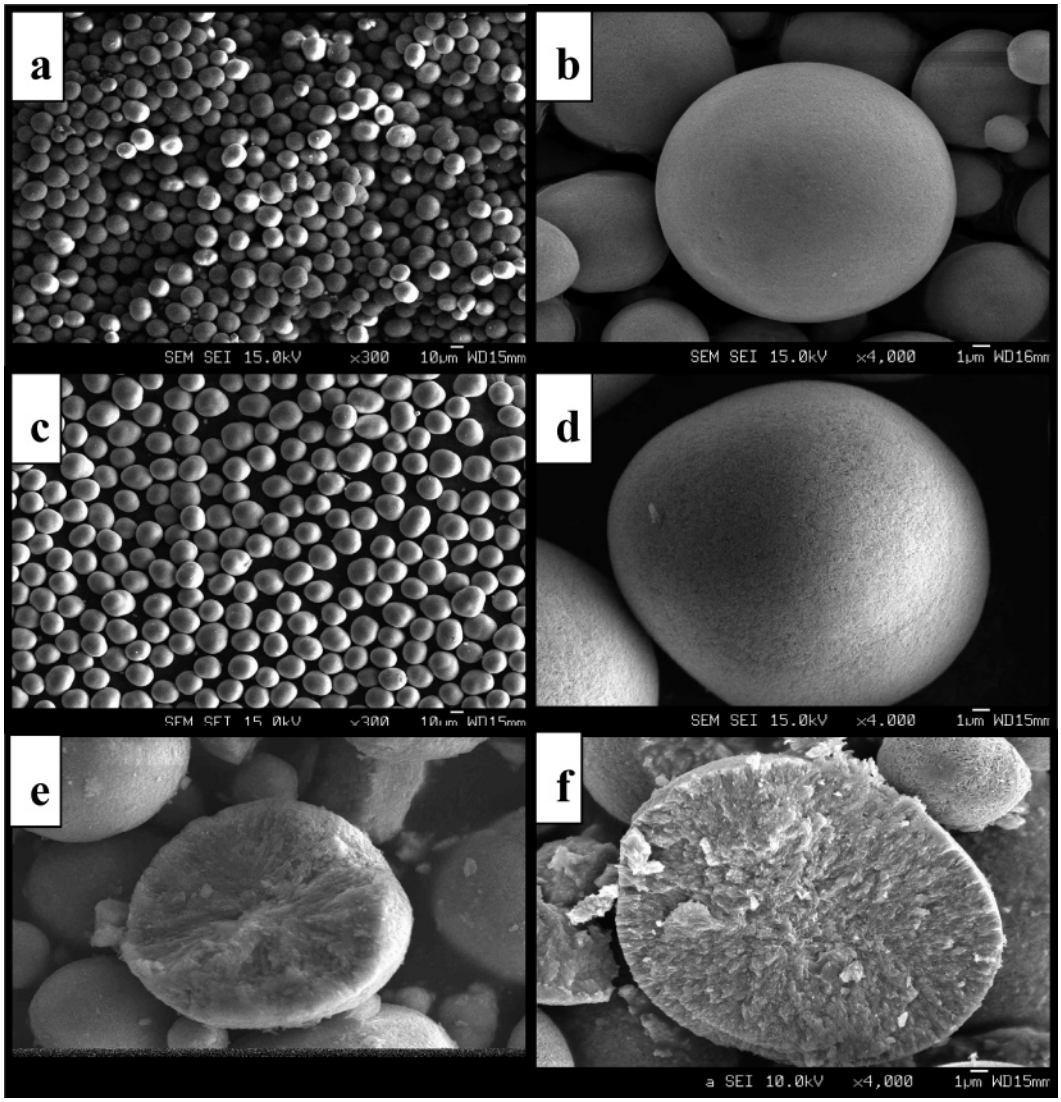

Figure 2. SEM images: (a) low- and (b) high-magnification of pristine $[Ni_{0.8}Co_{0.1}Mn_{0.1}](OH)_2$; (c) low- and (d) high-magnification of core−shell $[(Ni_{0.8}Co_{0.1}Mn_{0.1})_{0.8}(Ni_{0.5}Mn_{0.5})_{0.2}](OH)_2$; cross-section images of (e) $[Ni_{0.8}Co_{0.1}Mn_{0.1}](OH)_2$ and (f) $[(Ni_{0.8}Co_{0.1}Mn_{0.1})_{0.8}(Ni_{0.5}Mn_{0.5})_{0.2}](OH)_2$.

two dense parts, the core and shell. The thickness of the disjoined crust is about 1 μm. As shown in Scheme 1 (Step II), we expected that, if the $[Ni_{0.8}Co_{0.1}Mn_{0.1}](OH)_2$ is completely surrounded by the $[Ni_{0.5}Mn_{0.5}](OH)_2$, the particle size of the core−shell structured $[(Ni_{0.8}Co_{0.1}Mn_{0.1})_{0.8}(Ni_{0.5}Mn_{0.5})_{0.2}](OH)_2$ would be larger than that of the $[Ni_{0.8}Co_{0.1}Mn_{0.1}](OH)_2$. The particle size of $[(Ni_{0.8}Co_{0.1}Mn_{0.1})_{0.8}(Ni_{0.5}Mn_{0.5})_{0.2}](OH)_2$ is slightly greater than that of $[Ni_{0.8}Co_{0.1}Mn_{0.1}](OH)_2$ due to the presence of the $[Ni_{0.5}Mn_{0.5}](OH)_2$ shell, which indicates that $[Ni_{0.8}Co_{0.1}Mn_{0.1}](OH)_2$ is completely enclosed by the thick $[Ni_{0.5}Mn_{0.5}](OH)_2$ layer, resulting in the successful formation of the core−shell structured $[(Ni_{0.8}Co_{0.1}Mn_{0.1})_{0.8}(Ni_{0.5}Mn_{0.5})_{0.2}](OH)_2$.

The synthesized $[(Ni_{0.8}Co_{0.1}Mn_{0.1})_{0.8}(Ni_{0.5}Mn_{0.5})_{0.2}](OH)_2$ was fired with a stoichiometric amount of lithium at 770 °C for 20 h in air. Lower temperature calcination resulted in a lower crystallinity, while firing at a much higher temperature gave rise to severe cation mixing; the optimum temperature was 770 °C in our experiment. For comparison, $Li[Ni_{0.8}Co_{0.1}Mn_{0.1}]O_2$ was also synthesized by the calcination of $[Ni_{0.8}Co_{0.1}Mn_{0.1}](OH)_2$ and a LiOH mixture at 750 °C for 12 h in air. The corresponding XRD patterns appear in Figure 3. Simple heat

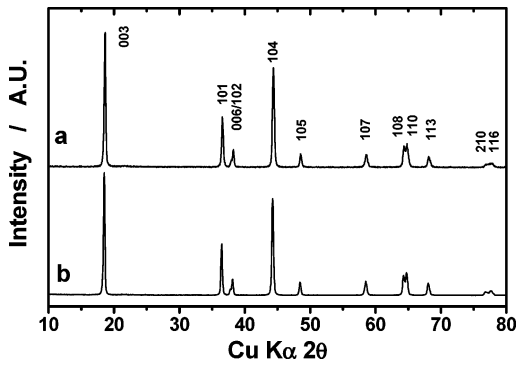

Figure 3. XRD patterns of (a) core−shell $Li[(Ni_{0.8}Co_{0.1}Mn_{0.1})_{0.8}(Ni_{0.5}Mn_{0.5})_{0.2}]O_2$ and (b) $Li[Ni_{0.8}Co_{0.1}Mn_{0.1}]O_2$ powders.

treatments of the hydroxides with a lithium salt brought about a well-ordered layer structure having a $R\bar{3}m$ space group for both cases in Figure 3. A chemical analysis of the final product obtained from the calcination of the lithium salt and the $[(Ni_{0.8}Co_{0.1}Mn_{0.1})_{0.8}(Ni_{0.5}Mn_{0.5})_{0.2}](OH)_2$ mixture yielded $Li[Ni_{0.74}Co_{0.08}Mn_{0.18}]O_2$, which can be rewritten by following the core−shell structure composition, $Li[(Ni_{0.8}Co_{0.1}Mn_{0.1})_{0.8}(Ni_{0.5}Mn_{0.5})_{0.2}]O_2$. Due to the similarity in its structure to

Table 1. Comparison of Lattice Parameters of Li[Ni$_{0.8}$Co$_{0.1}$Mn$_{0.1}$]O$_2$, Li[(Ni$_{0.8}$Co$_{0.1}$Mn$_{0.1}$)$_{0.8}$(Ni$_{0.5}$Mn$_{0.5}$)$_{0.2}$]O$_2$, and Li[Ni$_{0.5}$Mn$_{0.5}$]O$_2$

	a/Å	*c*/Å	volume/Å^3
Li[Ni$_{0.8}$Co$_{0.1}$Mn$_{0.1}$]O$_2$	2.8771(3)	14.2460(5)	102.125(10)
Li[(Ni$_{0.8}$Co$_{0.1}$Mn$_{0.1}$)$_{0.8}$(Ni$_{0.5}$Mn$_{0.5}$)$_{0.2}$]O$_2$	2.8813(7)	14.2747(12)	102.629(11)
Li[Ni$_{0.5}$Mn$_{0.5}$]O$_2$	2.8866(12)	14.2919(6)	103.134(7)

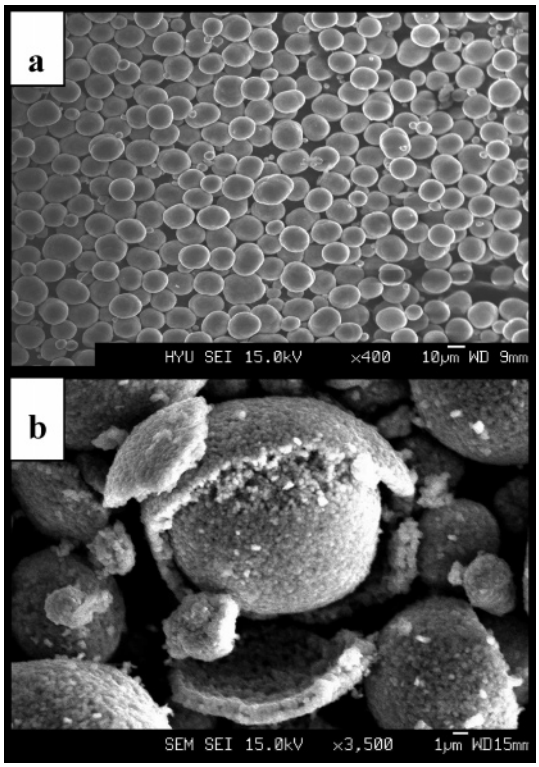

Figure 4. SEM images of (a) core−shell Li[(Ni$_{0.8}$Co$_{0.1}$Mn$_{0.1}$)$_{0.8}$(Ni$_{0.5}$Mn$_{0.5}$)$_{0.2}$]O$_2$ and (b) Li[Ni$_{0.8}$Co$_{0.1}$Mn$_{0.1}$]O$_2$ powders.

Li[Ni$_{0.8}$Co$_{0.1}$Mn$_{0.1}$]O$_2$, the XRD pattern of Li[(Ni$_{0.8}$Co$_{0.1}$Mn$_{0.1}$)$_{0.8}$(Ni$_{0.5}$Mn$_{0.5}$)$_{0.2}$]O$_2$ overlaps the Li[Ni$_{0.8}$Co$_{0.1}$Mn$_{0.1}$]O$_2$ core and the Li[Ni$_{0.5}$Mn$_{0.5}$]O$_2$ shell, so that the corresponding XRD pattern appears without a secondary phase. However, there is a tiny difference in a and b of Figure 3; the peak split between the (210) and (116) peaks for Li[Ni$_{0.8}$Co$_{0.1}$Mn$_{0.1}$]O$_2$ is clear in Figure 3b. The splitting for the core−shell structured Li[(Ni$_{0.8}$Co$_{0.1}$Mn$_{0.1}$)$_{0.8}$(Ni$_{0.5}$Mn$_{0.5}$)$_{0.2}$]O$_2$ is not as clear as that of Li[Ni$_{0.8}$Co$_{0.1}$Mn$_{0.1}$]O$_2$ in Figure 3a. Therefore, the Li[Ni$_{0.8}$Co$_{0.1}$Mn$_{0.1}$]O$_2$ and Li[(Ni$_{0.8}$Co$_{0.1}$Mn$_{0.1}$)$_{0.8}$(Ni$_{0.5}$Mn$_{0.5}$)$_{0.2}$]O$_2$ phases separately exist. Assuming a single phase, the lattice parameters were calculated based on the space group $R\bar{3}m$ (Table 1). The lattice parameters for the core−shell structure were somewhat higher than those of Li[Ni$_{0.8}$Co$_{0.1}$Mn$_{0.1}$]O$_2$. The calculated lattice parameters for Li[Ni$_{0.5}$Mn$_{0.5}$]O$_2$ are somewhat greater than those for the Li[Ni$_{0.8}$Co$_{0.1}$Mn$_{0.1}$]O$_2$ (Table 1). Therefore, it is possible that the Li[Ni$_{0.8}$Co$_{0.1}$Mn$_{0.1}$]O$_2$ core surrounded by the Li[Ni$_{0.5}$Mn$_{0.5}$]O$_2$ shell had slightly greater lattice parameters compared to Li[Ni$_{0.8}$Co$_{0.1}$Mn$_{0.1}$]O$_2$.

SEM observations of the produced Li[(Ni$_{0.8}$Co$_{0.1}$Mn$_{0.1}$)$_{0.8}$(Ni$_{0.5}$Mn$_{0.5}$)$_{0.2}$]O$_2$ illustrate that the spherical morphology of the hydroxide was maintained even after high-temperature calcination (Figure 4a). The estimated average particle diameter was about 15 μm. However, one critical concern is that firing at higher temperatures can bring about interatomic diffusion in the particulate, so that the core−shell structure would disappear by calcination.

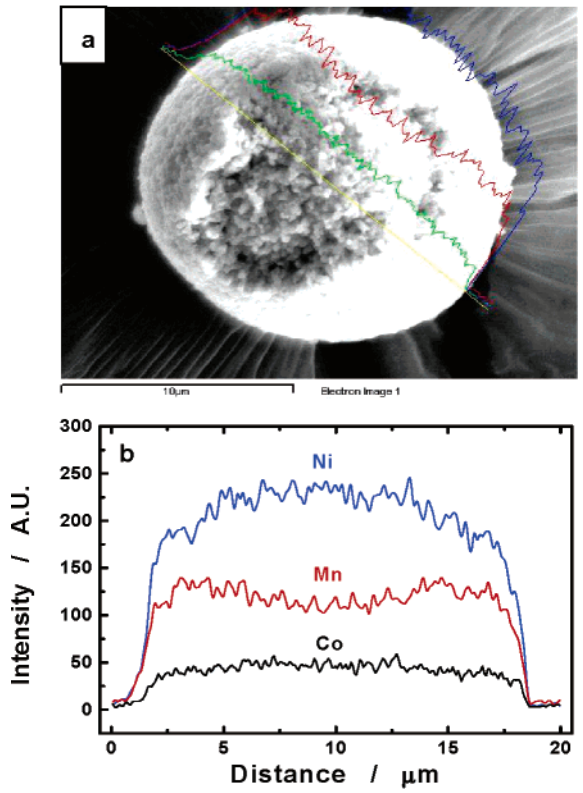

Figure 5. The energy dispersive spectroscopic (EDS) image of the Li[(Ni$_{0.8}$Co$_{0.1}$Mn$_{0.1}$)$_{0.8}$(Ni$_{0.5}$Mn$_{0.5}$)$_{0.2}$]O$_2$ particle.

The produced Li[(Ni$_{0.8}$Co$_{0.1}$Mn$_{0.1}$)$_{0.8}$(Ni$_{0.5}$Mn$_{0.5}$)$_{0.2}$]O$_2$ particles were partially crushed in an agate mortar to uncover whether the core−shell structure is preserved or destroyed after high-temperature calcination. Surprisingly, the core−shell structure was maintained after the calcination at a high temperature (Figure 4b). The particles showed the existence of a core and shell, as expected in Scheme 1 (Step III). The thickness of the broken crust was about 1−1.5 μm. We concluded from these results that the core−shell structure was maintained even after high-temperature calcination.

However, we doubted that the elemental diffusion from the core to the shell and/or the shell to the core would be inevitable during the high-temperature calcination because of the different compositions of the core and shell (which would lead to interatomic diffusion). Such an unsteady diffusion state is mainly due to the different concentration gradients at the boundary. Figure 5 shows the energy dispersive spectroscopic (EDS) results of the shell-broken Li[(Ni$_{0.8}$Co$_{0.1}$Mn$_{0.1}$)$_{0.8}$(Ni$_{0.5}$Mn$_{0.5}$)$_{0.2}$]O$_2$ particle. The analysis was done at the yellow line in Figure 5a. In the center part (the core) between 5 and 15 μm (Figure 5b), Ni and Co elements appear in abundance compared to those elements in the shell, while the Mn availability was relatively poor. This is natural because the core mainly consists of the Li[Ni$_{0.8}$Co$_{0.1}$Mn$_{0.1}$]O$_2$ phase. The Co component in the shell can diffuse to the surface of the core−shell particle with a concentration gradient from the Li[Ni$_{0.8}$Co$_{0.1}$Mn$_{0.1}$]O$_2$ core, so

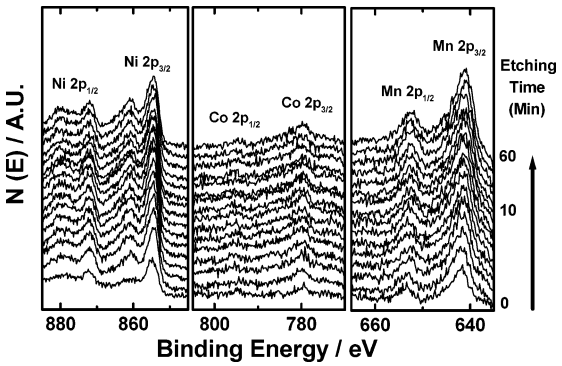

Figure 6. X-ray photoelectron spectroscopy (XPS) data of the core−shell structured $Li[(Ni_{0.8}Co_{0.1}Mn_{0.1})_{0.8}(Ni_{0.5}Mn_{0.5})_{0.2}]O_2$ particles.

a possible concentration gradient is likely to occur for the Co in $Li[(Ni_{0.8}Co_{0.1}Mn_{0.1})_{0.8}(Ni_{0.5}Mn_{0.5})_{0.2}]O_2$.

X-ray photoelectron spectroscopy (XPS) was employed to observe the surface elemental distribution of the core−shell structured $Li[(Ni_{0.8}Co_{0.1}Mn_{0.1})_{0.8}(Ni_{0.5}Mn_{0.5})_{0.2}]O_2$ particles (Figure 6). The Ni2p and Mn2p spectra can be seen in Figure 6 (before etching by Ar^+ ions). The Co2p spectrum is hardly observable. This suggests that the atomic concentration of Co seems to be negligible on the surface of the core−shell structure of the $Li[(Ni_{0.8}Co_{0.1}Mn_{0.1})_{0.8}(Ni_{0.5}Mn_{0.5})_{0.2}]O_2$. The intensity for Co became gradually higher than all the elements upon Ar^+ ion etching with the increasing sputtering time. Sputtering for 1 h (150 nm depth from the surface) resulted in a slightly increased intensity of Co and Mn (Figure 6). As we expected, the concentration gradient occurs for the Co in our experiment because the total amount of that element is poor in the final product, $Li[(Ni_{0.8}Co_{0.1}Mn_{0.1})_{0.8}(Ni_{0.5}Mn_{0.5})_{0.2}]O_2$, and that exists only in the core in the core−shell hydroxide so that the high-temperature calcination led to Co diffusion from the core to the shell that reached equilibrium in $Li[(Ni_{0.8}Co_{0.1}Mn_{0.1})_{0.8}(Ni_{0.5}Mn_{0.5})_{0.2}]O_2$. We also observed that the calcinations of the lithiated core−shell powders at 400 °C produced a shell containing negligible or no cobalt, which implies that the driving force for the cobalt diffusion is calcinations. Furthermore, the observed shifts of the binding energies are related to the difference in the oxidation state of the transition metal elements. The valences of Ni, Co, and Mn are believed to be +3 for the core $Li[Ni_{0.8}Co_{0.1}Mn_{0.1}]O_2$.[28] $Li[Ni_{0.5}Mn_{0.5}]O_2$ consists of Ni^{2+} and Mn^{4+} in its formal charge. The average oxidation state of Ni in the final products is +2 because the difference in the binding energy between $2p_{3/2}$ and $2p_{1/2}$ is approximately 17.5 eV even after an hour of etching (150 nm from the surface), which is indicative of divalent Ni.[29] This means that Ni diffusion would hardly occur from the shell to the core and/or from the core to the shell because the concentration of the Ni is rich in the core and shell. For the Mn, the difference in the binding energy between $2p_{3/2}$ and $2p_{1/2}$ was about 11.7 eV before etching (Figure 6).

However, the gap was reduced to approximately 9.4 eV after etching for 1 h (150 nm from the surface), which means that the average oxidation state of Mn has partially changed from +4 to +3 mainly due to the trivalent Co diffusion to the shell from the $Li[Ni_{0.8}Co_{0.1}Mn_{0.1}]O_2$ core. Hence, a small amount of Co-doped $Li[Ni_{0.5}Mn_{0.5}]O_2$ was formed in the inner part of the shell. Due to the analytical difficulty, it is presently impossible to clarify the detailed chemical compositions of each core and shell of $Li[(Ni_{0.8}Co_{0.1}Mn_{0.1})_{0.8}(Ni_{0.5}Mn_{0.5})_{0.2}]O_2$. From the above results, the core−shell structured $Li[(Ni_{0.8}Co_{0.1}Mn_{0.1})_{0.8}(Ni_{0.5}Mn_{0.5})_{0.2}]O_2$ is composed of the $Li[Ni_{0.5}Mn_{0.5}]O_2$ shell with a Co concentration gradient and the $Li[Ni_{0.8}Co_{0.1}Mn_{0.1}]O_2$ core.

We also studied the electrochemical properties of the core−shell $Li[(Ni_{0.8}Co_{0.1}Mn_{0.1})_{0.8}(Ni_{0.5}Mn_{0.5})_{0.2}]O_2$ compared to the $Li[Ni_{0.8}Co_{0.1}Mn_{0.1}]O_2$. Earlier reports suggested the that enhanced electrochemical properties of $Li[Ni_{1-x}M_x]O_2$ (M = Al, Co, Mn) used heterometal oxide coatings.[14,15] The coating layer, however, was only about a few nanometers thick and electrochemically inactive. In our study, the $Li[Ni_{0.8}Co_{0.1}Mn_{0.1}]O_2$ core was completely encapsulated by the microscale $Li[Ni_{0.5}Mn_{0.5}]O_2$ shell that participates in the electrochemical reaction by Li^+ intercalation/deintercalation. The distinct electrochemical properties of the core−shell particles are interesting. Coin-type cells using $Li[Ni_{0.8}Co_{0.1}Mn_{0.1}]O_2$ and/or $Li[(Ni_{0.8}Co_{0.1}Mn_{0.1})_{0.8}(Ni_{0.5}Mn_{0.5})_{0.2}]O_2$ as the positive electrode and Li metal as the negative electrode were used in the electrochemical experiments. They were charged and discharged at a constant current density of 40 mA/g, and the corresponding initial charge−discharge curves are in Figure 7. The $Li/Li[Ni_{0.8}Co_{0.1}Mn_{0.1}]O_2$ cell exhibited a discharge capacity of 200 mAh/g in the voltage range of 3.0−4.3 V, similar to the values in the literature.[15] Meanwhile, the $Li/Li[(Ni_{0.8}Co_{0.1}Mn_{0.1})_{0.8}(Ni_{0.5}Mn_{0.5})_{0.2}]O_2$ cell delivered a slightly lower specific discharge capacity, approximately 188 mAh/g. The $Li/Li[Ni_{0.8}Co_{0.1}Mn_{0.1}]O_2$ and $Li/Li[(Ni_{0.8}Co_{0.1}Mn_{0.1})_{0.8}(Ni_{0.5}Mn_{0.5})_{0.2}]O_2$ cells showed a similar initial charge and discharge efficiency of about 87−89%. In previous studies, $Li[Ni_{0.5}Mn_{0.5}]O_2$ usually showed a discharge capacity of ca. 150 mAh/g in the range of 3.0−4.3 V.[6,30,31] Therefore, it is reasonable to believe that the presence of $Li[Ni_{0.5}Mn_{0.5}]O_2$ as the shell reduces the total gravimetric capacity of the $Li[(Ni_{0.8}Co_{0.1}Mn_{0.1})_{0.8}(Ni_{0.5}Mn_{0.5})_{0.2}]O_2$. The operating voltage during the charge for the core−shell particle is almost 0.1 V higher than that of $Li[Ni_{0.8}Co_{0.1}Mn_{0.1}]O_2$ over the whole voltage range. Such a phenomenon can be ascribed to the intrinsic property of $Li[Ni_{0.5}Mn_{0.5}]O_2$, which has a relatively higher resistance than $Li[Ni_{0.8}Co_{0.1}Mn_{0.1}]O_2$. The polarization at lower voltages (<3.8 V) between the charge and discharge was also greater for the core−shell structured $Li[(Ni_{0.8}Co_{0.1}Mn_{0.1})_{0.8}(Ni_{0.5}Mn_{0.5})_{0.2}]O_2$ (Figure 7). The relatively steep voltage drop at the end of the discharge is also a typical voltage profile for $Li[Ni_{0.5}Mn_{0.5}]O_2$. Again, the core−shell particle is composed of the $Li[Ni_{0.8}Co_{0.1}Mn_{0.1}]O_2$ inner core and $Li[Ni_{0.5}Mn_{0.5}]O_2$ outer shell. The Li^+ deintercalation reaction begins from the surface of the shell in the core−shell particle. This means that Li^+ ions are extracted from the $Li[Ni_{0.5}Mn_{0.5}]O_2$ outer shell. As soon as all of the Li^+ ions are deintercalated from the outer shell, further extractions of Li^+ ions continued from the inner core. An inverse behavior would occur during the intercalation process. Therefore, it is likely that the larger

(28) Johnson, C. S.; Kropf, A. J. In situ XAFS analysis of the $Li_xNi_{0.8}Co_{0.2}O_2$ cathode during cycling in lithium batteries. *Electrochim. Acta* **2002**, *47*, 3187−3194.
(29) Wagner, C. D.; Riggs, W. M.; Davis, L. E.; Moulder, F. F.; Muilenberg, G. E. *Handbook of X-ray Photoelectron Spectroscopy*; Perkin-Elmer, Eden Praire, MN, 1978; pp 60−100.
(30) Sun, Y.-K.; Kang, S.-H.; Amine, K. Synthesis and electrochemical behavior of layered $Li(Ni_{0.5-x}Co_{2x}Mn_{0.5-x})O_2$ (x = 0 and 0.025) materials prepared by solid-state reaction method. *Mater. Res. Bull.* **2004**, *39*, 819−825.
(31) Myung, S.-T.; Lee, M.-H.; Park, S.-H.; Sun, Y.-K. Hydrothermal synthesis of layered $Li[Ni_{0.5}Mn_{0.5}]O_2$ as lithium intercalation material. *Chem. Lett.* **2004**, *33*, 818−819.

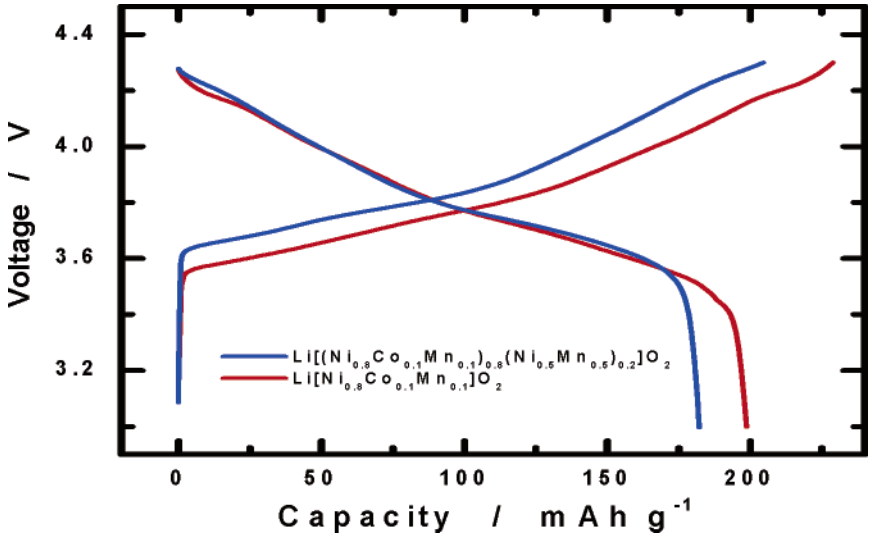

Figure 7. The initial charge–discharge curves of $Li/Li[Ni_{0.8}Co_{0.1}Mn_{0.1}]O_2$ and $Li/Li[(Ni_{0.8}Co_{0.1}Mn_{0.1})_{0.8}(Ni_{0.5}Mn_{0.5})_{0.2}]O_2$ cell at the voltage range of 3.0–4.3 V.

polarization in the lower voltage region would be ascribed to the outer $Li[Ni_{0.5}Mn_{0.5}]O_2$ shell and the lower polarization at a higher voltage would be due to the inner $Li[Ni_{0.8}Co_{0.1}Mn_{0.1}]O_2$ core of the core–shell structured $Li[(Ni_{0.8}Co_{0.1}Mn_{0.1})_{0.8}(Ni_{0.5}Mn_{0.5})_{0.2}]O_2$.

To observe the long-term cycling properties, a carbon electrode was employed as the negative electrode. Laminated-type lithium ion batteries using an Al pouch with a capacity of approximately 120 mAh were assembled. The fabricated batteries were charged and discharged for 500 cycles at the rate of 1 C between 3.0 and 4.3 V. The $C/Li[Ni_{0.8}Co_{0.1}Mn_{0.1}]O_2$ battery has a capacity retention of 81% after 500 cycles (Figure 8). With cycling, the voltage at the beginning of the discharge gradually decreased. It also showed a slow decrease in the operating voltage (as much as 0.2 V at the 500th cycle), compared to the first discharge in Figure 8a; the structural instability and dissolutions of Co from the active material by a HF attack would deteriorate the long-term cycling stability.[32,33] The $C/Li[(Ni_{0.8}Co_{0.1}Mn_{0.1})_{0.8}(Ni_{0.5}Mn_{0.5})_{0.2}]O_2$ cell, however, has a superior cyclability with a capacity retention of 98% after 500 cycles (Figure 8c). The voltage difference during cycling is lower compared to $C/Li[Ni_{0.8}Co_{0.1}Mn_{0.1}]O_2$ (Figure 8b). In this case, the $Li[Ni_{0.5}Mn_{0.5}]O_2$ outer shell, which shows a stable cyclability in the same voltage range,[6,9–13,30,31] is associated with the cycling behavior improvement. If $Li[Ni_{0.8}Co_{0.1}Mn_{0.1}]O_2$ appears on the surface of the core–shell particles or exists as impurities in the final product, such extraordinary cycling behavior cannot be achieved due to the structural instability of $Li[Ni_{0.8}Co_{0.1}Mn_{0.1}]O_2$. Since the $Li[Ni_{0.5}Mn_{0.5}]O_2$ shell is completely surrounded by the $Li[Ni_{0.8}Co_{0.1}Mn_{0.1}]O_2$ core, it could prevent the potential HF attack of $Li[Ni_{0.8}Co_{0.1}Mn_{0.1}]O_2$ from the electrolyte during long-term cycling; Co dissolution could be suppressed and retain its capacity during the cycling.

It is well-known that $LiNiO_2$ and its derivatives suffer from thermal instability.[4,5] Therefore, we studied the thermal stability

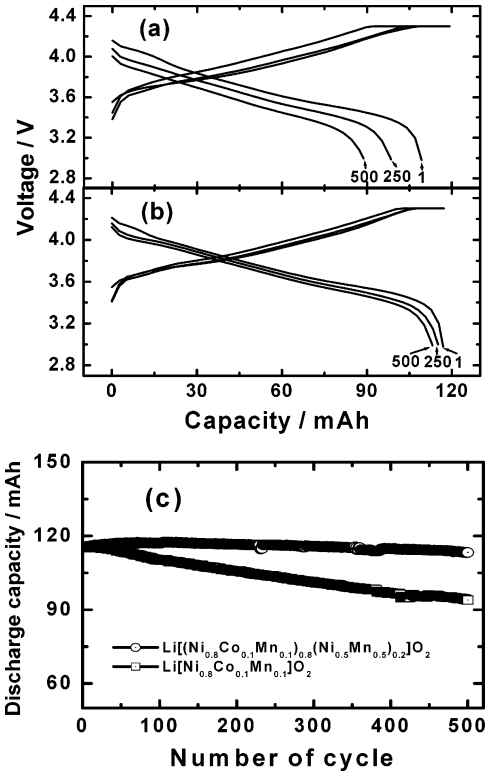

Figure 8. (a) Continuous charge–discharge curves of $C/Li[Ni_{0.8}Co_{0.1}Mn_{0.1}]O_2$ cell; (b) continuous charge–discharge curves of $C/Li[(Ni_{0.8}Co_{0.1}Mn_{0.1})_{0.8}(Ni_{0.5}Mn_{0.5})_{0.2}]O_2$ cell; (C) corresponding discharge capacity versus cycling number.

of the delithiated core–shell $Li[(Ni_{0.8}Co_{0.1}Mn_{0.1})_{0.8}(Ni_{0.5}Mn_{0.5})_{0.2}]O_2$ electrodes by differential scanning calorimetry (DSC) in the charged state to 4.3 V. Figure 9 shows that this electrode had a higher exothermic reaction onset temperature than the $Li[Ni_{0.8}Co_{0.1}Mn_{0.1}]O_2$ electrode. For the $Li[Ni_{0.8}Co_{0.1}Mn_{0.1}]O_2$ electrode, the onset temperature of an exothermic peak was about 180 °C, above which an abrupt exothermic reaction with the heat (3285 J/g) was observed at about 220 °C. Meanwhile, $Li[(Ni_{0.8}Co_{0.1}Mn_{0.1})_{0.8}(Ni_{0.5}Mn_{0.5})_{0.2}]O_2$ showed an exothermic reaction at 250 °C and had a reduced heat of 2261 J/g when compared with the $Li[Ni_{0.8}Co_{0.1}Mn_{0.1}]O_2$ electrode. $Li_{1-x}NiO_2$ is thermally

(32) Amatucci, G. G.; Tarascon, M. M.; Klein, L. C. Cobalt dissolution in $LiCoO_2$-based non-aqueous rechargeable batteries. *Solid State Ionics* **1996**, *83*, 167–173.
(33) Myung, S.-T.; Kumagai, N.; Komaba, S.; Chung, H.-T. Effects of Al doping on the microstructure of $LiCoO_2$ cathode materials. *Solid State Ionics* **2001**, *139*, 47–56.

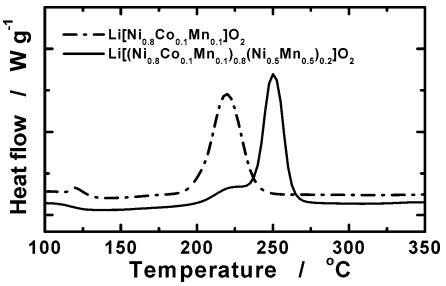

Figure 9. Differential scanning calorimetry (DSC) traces of $Li[(Ni_{0.8}Co_{0.1}Mn_{0.1})_{0.8}(Ni_{0.5}Mn_{0.5})_{0.2}]O_2$ and $Li[Ni_{0.8}Co_{0.1}Mn_{0.1}]O_2$ at charged state to 4.3 V.

unstable because of the oxygen release from the host structure.[5] As we previously reported, the exothermic temperature of $Li[Ni_{0.5}Mn_{0.5}]O_2$ itself is about 270−280 °C and has a reduced heat generation.[9,11] We think that the thermally stable outer $Li[Ni_{0.5}Mn_{0.5}]O_2$ shell suppresses the oxygen release from the highly delithiated $Li_{1-x}[Ni_{0.8}Co_{0.1}Mn_{0.1}]O_2$, thereby improving the thermal stability of $Li[(Ni_{0.8}Co_{0.1}Mn_{0.1})_{0.8}(Ni_{0.5}Mn_{0.5})_{0.2}]O_2$.

Conclusions

A $Li[(Ni_{0.8}Co_{0.1}Mn_{0.1})_{0.8}(Ni_{0.5}Mn_{0.5})_{0.2}]O_2$ containing a microscale spherical core−shell structure, that is, $LiNi_{0.8}Co_{0.1}Mn_{0.1}O_2$ as the core and a $Li[Ni_{0.5}Mn_{0.5}]O_2$ as the shell, was synthesized and characterized for its morphological and electrochemical properties. A high capacity was delivered from the $LiNi_{0.8}Co_{0.1}Mn_{0.1}O_2$ core, while the high thermal stability stemmed from the $Li[Ni_{0.5}Mn_{0.5}]O_2$ shell. The $Li[(Ni_{0.8}Co_{0.1}Mn_{0.1})_{0.8}(Ni_{0.5}Mn_{0.5})_{0.2}]O_2$ cathode also exhibited excellent cyclability with a capacity retention of 98%, while the $Li[Ni_{0.8}Co_{0.1}Mn_{0.1}]O_2$ oxide cathode without the $Li[Ni_{0.5}Mn_{0.5}]O_2$ shell produced capacity retention of only 81% in Li ion cells after 500 cycles. The thermal stability of the fully charged $Li[(Ni_{0.8}Co_{0.1}Mn_{0.1})_{0.8}(Ni_{0.5}Mn_{0.5})_{0.2}]O_2$ cathode was found to be significantly better than the $LiNi_{0.8}Co_{0.1}Mn_{0.1}O_2$ oxide cathode. The core−shell structured $Li[(Ni_{0.8}Co_{0.1}Mn_{0.1})_{0.8}(Ni_{0.5}Mn_{0.5})_{0.2}]O_2$ as a new positive electrode material is a significant breakthrough in the development of high-capacity lithium batteries. The synergetic effects of the microscale core−shell particles as lithium storage materials can open a new era for the development of advanced Li ion batteries with a high energy density, long cycle life, and safety. The core−shell concept can also be extended to the synthesis of several new useful intercalation compounds.

Acknowledgment. This work was supported by the Ministry of Information & Communications, Korea, under the Information Technology Research Center (ITRC) Support Program.

Supporting Information Available: XRD, DSC, and SEM image for various core−shell materials. This material is available free of charge via the Internet at http://pubs.acs.org.

JA053675G